Analyst

Accepted Manuscript

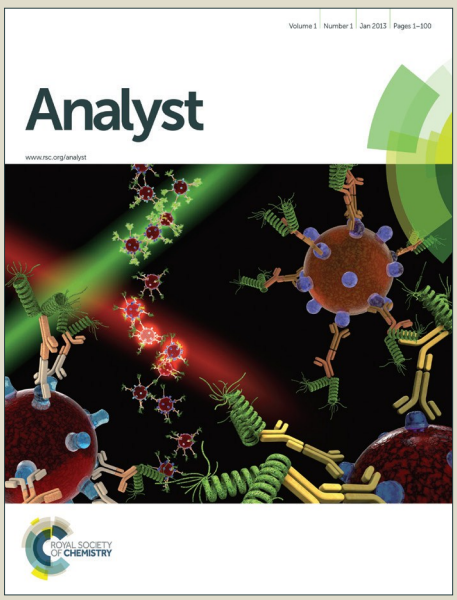

ROYAL SOCIETY OF CHEMISTRY

www.rsc.org/analyst

Eicosyl ammoniums elicited thermal reduction alleyway towards gold nanoparticles and their chemo-sensor aptitude

Dolly Rana[a], Deepika Jamwal[a], Akash Katoch[b], Pankaj Thakur[*a,c], Susheel Kalia[d],

[a] *School of Chemistry, Faculty of Basic Sciences, Shoolini University, Solan (HP)-173212, India.*

[b] *Institute Instrumentation Centre, Indian Institute of Technology Roorkee, Roorkee - 247667, India.*

[c] *Istituto Italiano Di Tecnologia (Centre for Advanced Biomaterials for Healthcare) Naples 80125, Italy.*

[d] *Department of Chemistry, Army Cadet College Wing, Indian Military Academy, Dehradun –248007 (UK) India.*

[*] *Corresponding author*: *Pankaj.thakur@iit.it, chempank@gmail.com*

The construction of dimethylenebis(eicosyldimethylammonium bromide) surfactant directed gold nanoparticles have been accomplished via one-pot thermal reduction of $HAuCl_4$ with trisodium citrate. The effect of cationic twin tail surfactants dimethylenebis(hexadecyldimethylammonium bromide) (16-2-16), dimethylenebis-(octadecyldimethylammonium bromide) (18-2-18) and dimethylenebis-(eicosyldimethylammonium bromide) (20-2-20) and their concentrations on shape and size of Au nanoparticles was thoroughly investigated. The UV-Vis spectroscopy and transmission electron microscopy (TEM) result spectacles that higher tail length surfactants act as shape directing agents promoting diversified morphologies. The formation of multiple-shaped Au nanoparticles such as round, hexagon, pentagon, triangular and rod has been confirmed from microstructures analysis; amongst, the expanse of triangular shapes enhanced at elevated levels of concentration surfactants. In addition, the triangular Au nanoparticles with truncated corners were changed to smooth corner as the hydrocarbon chain length increased from (18-2-18) to (20-2-20). The concentration and hydrocarbon tails of twin tail surfactant strongly influences the size and structure of Au NPs. In addition, the prepared Au NPs synthesized with twin tail surfactant (18-2-18) were found highly sensitive towards Hg^{2+}, which could be because of the preferential adsorption of Hg^0 on lower energy facets of triangular shape Au NPs.

1. Introduction

Anisotropic nanostructure of noble metals such as Au, Ag, Pt etc have manifested their utility in distinct applications such as catalysis, nanoscale electronic, optical devices, bio- or chemosensors, biomedicines and other areas.[1-3] Eventually, all these solicitations strongly hinge on the control and design of the size, shape and dimensional anisotropy of the architecture blocks which are significantly different from those of the corresponding bulk materials. Specific brand of shape and size with high yield controlled metal-nanostructure can be achieved by varying the different reaction parameters in various synthetic routes which is alternative tool to adjust optical or structural properties of the materials.

Heretofore, anisotropic nanostructures of noble metals have been successfully synthesized including 1D nanostructure (nanowires, nanorods, nanotubes), 2D nanostructure (nanoplates, nanosheets, nanoribbons) and 3D nanostructure (nanocubes, nanostars, nanoflower)[4-6] by using conventional surfactant such as cetyltrimethylammonium bromide (CTAB), sodium dodecyl sulfate (SDS), polyvinylpyrrolidone (PVP) and mixed surfactant system and common stabilizers like polymers, dendrimers, biomolecules, plant extract.[7-11] Among them, conventional surfactants have been proved as good soft template for the high yield synthesis of anisotropic nanostructure with high reproducibility. Cationic twin tail surfactants inherit very low critical micelle concentration (cmc) values in comparison to conventional surfactants. In addition, they show excellent adsorption ability at the liquid-solid interface because of their high hydrophobic character, thereby controls growth of nanomaterials.[12,13] A variety of methods including Turkevich method,[12]seed-mediated growth,[14-17] hydrothermal process,[18] water-in-oil reverse micelles system,[19] template synthesis,[20] room temperature synthesis,[21] microemulsions[22] have so far used to synthesize anisotropic nanostructure of metal and semiconductor nanoparticles with twin tail surfactants (TTS).

According to previous studies, the TTS significantly influenced the shape and size of nanomaterials.[16,23,24] A few studies have been conducted to investigate the effect of higher TTS by changing chain or spacer length, structure variation in head and tail groups.[14, 25-28] The specific capping agent adsorb on low energy crystal facets selectively and reduce their involvement in the nucleation process that explicit the crystal growth at uncapped or poorly capped high energy crystal facets to attain desired morphologies.[29] For example, 1D Au well-defined nanoribbons of several micrometers long were synthesized by seed- growth method using dimethylenebis(tetradecyldimethylammonium bromide) (14-2-14). A preferential adsorption of (14-2-14) on the higher energy {100} facets results in subsequent growth in the {011} direction enclosed by {111} planes.[16] Another study,[23] evaluated the effect of gemini surfactant on shape controlled synthesis of Au NPs by comparing the capping ability of didodecyldimethylammonium bromide (12-0-12) and hexamethylene-1, 6-bis-(dodecyldimethylammonium bromide) (12-6-12). The alteration in steric hindrances due to change in spacer length resulted in symmetric to anisotropic growth of Au NPs. However, most of studies are limited to the use of smaller chain lengths and predominantly the effect of longer hydrocarbon chain length on shape and size of Au NPs have rarely been investigated. Thus, further investigations are required to explain the significance of longer hydrocarbon chain length for the synthesis of metal NPs.

Previously, metal NPs has widely been used for the detection of heavy metal ions, drugs, cancerous cells, small biomolecules, melamine.[30-35] Particularly, metal NPs with specific shape have been center of attraction for chemosensor applications not only because of their physical and chemical properties but also due to growth of low energy facets that act as preferential absorption sites for interfacial interaction between metal NP and heavy metal ions.[36-38]

Consequently, usage of these nanostrucutres may be operative to improve detection of heavy metal ions.

Considering the aforementioned implication, we have selected a series of cationic TTS with longer hydrocarbon chain lengths (abbreviated as (*m-2-m*) (*m*=16, 18, 20)) in relation to their different concentrations for the synthesis of Au NPs. A novel and eicosyldimethyl twin-tail surfactants mediated approach has been adopted to synthesize Au NPs with anisotropic shapes by a simple one-pot thermal reduction method. Further, the chemo-sensing activity of the respective Au NPs to detect Hg^{2+} has also been demonstrated. The results reveal that both hydrocarbon chain length and their concentration greatly influence the shape and size of Au NPs and there is a need to optimize the same, additionally, the detection of Hg^{2+} has been found to rely on the shape of Au NPs.

2. Experiments

2.1 Reagents

The Au precursor, chloroauric acid ($HAuCl_4$, Sigma Aldrich), sodium citrate tribasic dihydrate ($C_6H_5O_7\ Na_3.\ 2H_2O$) have been procured from Sigma Aldrich. The TTS with different hydrocarbon chain lengths; dimethylenebis(hexadecyldimethylammonium bromide) (16-2-16), dimethylenebis(octadecyldimethylammonium bromide) (18-2-18) and dimethylenebis (eicosyldimethylammonium bromide) (20-2-20) have been synthesized using procedure reported previously.[39]All the three surfactants were used after repeated crystallizations using mixture of acetone and ethyl acetate (1:1) as a solvent. Sodium acetate ($C_2H_3NaO_2$), hydrochloric acid (HCl), sodium hydroxide (NaOH), sodium chloride (NaCl) and all metal salts ($HgCl_2$, $RuCl_3.2H_2O$, $CdCl_2$, $Pb(C_2H_3O_2)$, $SnCl_2$, $NiCl_2$, $CuCl_2$, $ZnCl_2$, $FeCl_2$, and $MnCl_2$,) used in sensing measurement, were purchased from Sigma Aldrich. Double distilled water was used for

all preparations. The glassware were cleaned with freshly prepared HCl/HNO_3 (3:1, aquaregia), subsequently then rinsed thoroughly with double distilled water and dried in oven prior to use.

2.2 Characterizations

The prepared Au NPs have been characterized using UV-Visible spectroscopy (Systronics 2202 spectrophotometer) in the wavelength range of 450-900 nm to determine the absorbance due to surface plasmon resonance (SPR). The formation of Au NPs was monitored in the absorption range of 525-590 nm. The morphological analysis of Au NPs was performed using transmission electron microscope (TEM, Philips CM-200). Energy dispersive X-ray spectroscopy (EDXS), attached to the TEM equipment, have been used to investigate the chemical composition of Au NPs and the average size of Au NPs was collected from more than 100 particles. The Fourier transformed infrared spectroscopy (FTIR) of prepared Au NPs solutions were taken using Agilent Cary 630 100 V FTIR spectrometer, operated in range 700 -3000 cm^{-1}, respectively.

2.3 Synthesis of gold nanoparticles

For synthesis of the Au NPs, 50 mL aqueous solution of $HAuCl_4.3H_2O$ (0.25 mM) was boiled for 30 minutes at 110 ^oC. A freshly prepared aqueous sodium citrate (5.0 mL,2.5 mM) containing (16-2-16) TTS solution of concentration 0.10-5 mM was added in the gold salt solution and kept under vigorous stirring at 110 ^oC. Subsequently, the color of solution transformed directly from pale yellow color to ruby redcolor within 30 seconds. The reaction was allowed to proceed further for 30 minutes in order to produce a stable solution. The solution was then left undisturbed at room temperature for 2h. Also, the color of Au solution prepared without TTS first transformed from pale yellow to blue and then to ruby red in 15 minutes, respectively. The prepared Au NPs were washed with distilled water using centrifuge at 5,000 rpm in order to remove supernatant TTS and re-dispersed in distilled water. Similar procedure was employed to

synthesize Au NPs with TTS (18-2-18) and (20-2-20) with concentration 0.10-5 mM, respectively.

2.4 Au NPs as chemo-sensor for detection of Hg^{2+} ions

0.01 M $C_2H_3NaO_2$ buffer solution with pH range from 1.5 to 11 by 0.1 M HCl and NaOH was prepared. The sodium chloride (NaCl) was used to determine destabilization condition of Au NPs. The optimized NaCl concentration in aqueous Au NPs reduces the electrostatic repulsion between TTS-Au NPs and provides a low barrier for metal-ion-induced NP aggregation. Thereby, accomplish detection of very low concentrations of metal ions. The synthesized Au NPs (*m*=16, 18, 20) were stable in 1, 1.5 and 2 M of NaCl concentrations at pH 4, respectively. For detection of Hg^{2+}, 1500 µL aliquots of as prepared Au NPs were pre-treated with 500 µL of NaCl. The primed solution was then added to aqueous Hg^{2+} (in range from 10-450 µM) which was prepared in 0.01M sodium acetate buffer solution at pH 4.0.The resulting solution was left for several minutes at room temperature in order to determine preliminary sensing measurement though naked eye before UV-Vis analysis.

3. Results and discussion

3.1 UV-visible spectra

The UV-Vis spectra of Au NPs synthesized using TTS (*m*=16, 18, 20) with different concentrations are shown in Figs. 1(a), 1(c) and 1(e). The transverse surface Plasmon resonance (TSPR) peaks observed around 525-586 nm along with weak longitudinal surface Plasmon resonance (LSPR) peak around 742-856 nm is the characteristic of the collective conduction electrons with incident electromagnetic radiations. On the other hand, in the absence of TTS, only a sharp TSPR peak obtained at 530 nm (Fig. S1). Evidently, the red-shift in TSPR peak

transpired at elevated TTS concentration and analogous leaning has been witnessed for all the TTS indicating that the Au NPs size upsurge as a function of surfactant concentration.

For better understanding, the change in TSPR peak wavelength and intensity as function of TTS concentration have been summarized in Figs. 1(b), 1(d) and 1(f) respectively, which clearly displays that the TSPR peak and their intensity shifted towards higher wavelength proportionally with increase in concentration of TTS, which indicates an increase in size of Au NPs. It has also been noted that there is no LSPR observed in the Au NPs synthesized without TTS, which generally indicates the formation of monodispersed round shaped Au NPs.[23] On the other hand, UV-Vis spectra of the Au NPs synthesized with TTS consists of LSPR in the range from 742-856 nm, which is indicative of presence of Au NPs with different shapes. The presence of both TSPR and LSPR along with red-shift in absorbance peak clearly signposts that the TTS acts as shape directing negotiator for Au NPs, where shapes and size of Au NPs are strongly dependent on the length of hydrocarbon chain of the TTS.

A comparative absorbance spectra of Au NPs synthesized with 4 mM of TTS with different hydrocarbon chain length has also been demonstrated in Fig 2(a) evincing blue shift of about 24 nm in TSPR peak with increase in chain length of TTS from (16-2-16) to (20-2-20), which indicates that hydrocarbon chain length promotes the growth of Au NPs of specific shape. Virtually, somewhat comparable inclinations have been observed for other concentrations of TTS as well.

3.2 TEM measurements & morphology

In order to investigate the influence of hydrocarbon chain length of TTS and their concentration on shape and size of Au NPs, the microstructure of Au NPs have been examined by TEM analysis and the samples prepared with concentration 0.10 and 4 mM were selected for the same. The TEM images of Au NPs synthesized with concentrations 0.1 and 4mM of (16-2-16) have

been revealed in Figs. 3(a) and 3(c). Evidently, the Au NPs of different shapes including round, triangular, pentagon and hexagon were formed with 0.10 mM of (16-2-16) and additionally, the rectangular and rod shapes have been pragmatic as the concentration increases to 4mM. The yield of particles with different shapes for 0.10 and 4 mM of (16-2-16) have been summarized in Figs. 3(b) and 3(d). The numbers of round shape particles were decreased, whereas the triangular, shape slightly increased as the concentration increased to 4 mM.

The size distribution of particles is summarized in Figs.S2 (a) and S2 (b). The average size of Au NPs was increased from 39.6±13.0 to 54.8±25.5 nm with concentration of (16-2-16), which is mainly because of the growth of particles with different shape. Figs 3(e) and 3(f) show high resolution TEM image of triangular Au NPs (4 mM). Manifestly, the surface of Au NPs was covered by extremely thin layer of TTS (~ 1.4 nm) signifying thereby that the TTS continuously help in growth of Au NPs and act as shape directing agent. Further, the results of elemental line scans with respect to Au are displayed in Fig. 3(g) demonstrating that Au is distributed in the whole volume of an individual nanoparticle thereby deducing that Au is confined throughout region and confirms formation of Au NPs. Figure 3(h) shows EDS spectrum taken from Au NPs whereby the peak corresponding to Au is clearly observed in the spectrum. An additional peak of Cu was observed because of Cu grid used for sample preparation. The EDS spectral data of Au nanoparticles synthesized using different TTS are not shown here for avoiding redundancy.

The TEM images of Au NPs synthesized using 0.10 mM of (18-2-18) are shown in Fig. 4(a) and for 4mM are shown in Figs. 4(c) and 4(e). The corresponding particle size distribution and yield with different shapes are summarized in Figs. S2(c) & S2(d) and in Figs. 4(b) & 4(d), respectively. Palpably, the average size of NPs increased more than double from 66.6±36.5 nm and 138.4±71.4 nm for 0.10 and 4mM of (18-2-18). In addition, among different shapes of Au

NPs, the yield of triangular shape was increased by ~ 28 %. This clearly indicates that the longer hydrocarbon chain length of TTS significantly affects the shape and growth of Au NPs. Figure 4(f) shows the high magnification images of triangular shaped NPs, where the Au NPs comprises of truncated edges. The high magnification TEM images of corner region of triangular NPs from Fig. 4(f) are shown in Figs. 4(g) and 4(h). It can be seen that the surface of Au NP consists of surfactant layer of thickness ~ 1.7 nm.

The TEM images of Au NPs synthesized from 0.10 and 4 mM of (20-2-20) are shown in Figs. 5(a) and 5(c) and their corresponding size distribution and yield with different shapes are summarized in Figs.S2(e) and S2(f) and in Figs. 5(b) and 5(d), respectively. The Au NPs shape changed in similar way as occurred in the case of (18-2-18). The average size of Au NPs was 42.6±17.7 nm and 54.8±30.9 nm for 0.10mM and 4mM concentrations of surfactant, respectively. The yield of triangular shaped particles increased by ~ 20 % with an increase in surfactant concentration. However, the change in average size of Au NPs was marginal as compared to that of synthesized with (18-2-18). On the basis of these results, it is reasonable to conclude that the TTS concentration is one of important factor which need to be optimized in order to obtain desired size of NPs. The high magnification images of triangular Au NPs are shown in Figs. 5(e) and 5(f) where, the triangular shaped particles with smooth curvature were synthesized with (20-2-20) in comparison to the truncated corner observed with (18-2-18). In other words, the more number of growing corners are present in (18-2-18) Au NPs in comparison to other TTS capped NPs. Therefore, it can be inferenced that the hydrocarbon chain length of TTS has significant effect on the growth of Au NPs. The longer hydrocarbon chain of TTS promotes growth of NPs and lead to give triangular shaped NPs.

3.3 FTIR spectroscopic measurements and surface adsorption

The FTIR spectra of Au NPs synthesized using 4 mM concentration of TTS (m = 16, 18, 20) are revealed in Fig. 6. The FTIR of pure TTS included for assessment, are shown in Fig. S3. The peaks assigned at 2854, 2921 and 2925 cm^{-1}, respectively correspond to symmetric (ν_{sym}(C-H)) and anti-symmetric (ν_{asym} (C-H)) stretching vibrations of methylene group. The original NR_4^+ asymmetric bending (ρ_{asym} (NR_4^+)) peak at 1640 cm^{-1} related to all three TTS was shifted to 1659 cm^{-1} for all surfactant capped Au NPs. In addition, new peaks appeared at 1573 and 1585 cm^{-1} respectively, indicating the presence of higher density of gauche defects when surfactants molecules bind to Au surface.[40] The high frequency shift in scissoring vibration of the methylene chains (C-H) was observed for peaks at 1469 and 1473cm^{-1} to 1473 and 1477 cm^{-1}, which is indicative of more gauche defects. In addition, the peaks corresponds to asymmetric N-C bend ($\delta_s(N^+\text{-}(CH_3)_3)$) and band of the methyl rocking mode at 1394, 1398 and 855 cm^{-1} were shifted to1395, 1398 and 847, 840, 844 cm^{-1} indicates higher energy end-gauche defects than pure TTS[41,42] and suggests that the quaternary ammonium head group of surfactants is strongly attached with the gold surface.[43,44]

The twisting ($\rho_t(CH_2)_n$) and wagging vibrations ($\rho_w(CH_2)_n$) appeared at 1268, 1302, 1305 and 1302 cm^{-1} for pure TTS was shifted to (1275, 1309), (1261, 1298), (1264, 1298) cm^{-1} respectively. All the twin tail capped Au NPs exhibit R_T (trans C-C bond) and R_G (gauche C-C bond) modes at 1160, 1138 and 1082 cm^{-1} respectively, which is indicative of either a near-surface defect or an internal kink in the TTS capping layer covered on the surface of Au NPs.[45] The higher frequency shifts in rocking mode of the methylene chain $\rho_r(CH_2)_n$ in the presence of Au NPs indicate that surfactants have lost their crystalline nature. The peaks positions in relation to the TTS are summarized in Table 1. The FTIR result confirms that the Au NPs were capped with TTS and supports the results obtained by TEM analysis. High magnification TEM images

divulge the thickness of capped surfactant layer to be very much comparable to the single layer of surfactant monomers.[27] And also that the particles were well dispersed without any agglomeration, which is likely to be due to the hydrophobic character of TTS present on the surface of Au NPs. Moreover, the higher concentration of TTS is likely to have more interfacial adsorption, which would control the shape and size more effectively.

The shape transformation occurring from round to hexagon to triangular, may be a consequence of preferential adsorption of surfactant molecules on the low energy (111) plane of Au face centered cube (fcc) geometry[29] and restrict growth along (111) direction whereas promotes growth along six (110)-type directions and (110) plane, as illustrated in Scheme 1. Likewise, the shape and size of Au NPs changed in following trend: round < hexagon < triangular, as a function of surfactant hydrocarbon chain length and concentration. The transformation of shape from hexagon to triangular is well discussed in previous reports.[46,47] The TTS with longer hydrocarbon chain is likely to cover surface more effectively and promote additional liquid-solid interfacial adsorption resulting in the growth of Au NPs. Supplementary surfactant adsorbed on the surface of Au NPs subsequently promotes growth of NPs and the average of Au NPs size in relation with different shapes is summarized in Table 2. The particles size obtained from (18-2-18) was much higher in comparison to other TTS. Particularly, longer hydrocarbon chain in (20-2-20) has low impact on particles size, whereas, triangular particles with smooth round corners were prepared. This suggests that the long hydrocarbon chain promotes faster NPs growth in comparison to surfactants with small length hydrocarbon chains.

3.4 Chemo-sensing aspect

Auxiliary, the prepared Au NPs have also been used as probe for detection of Hg^{2+}.In order to optimize sensing conditions and estimate detection limit of Hg^{2+}, varying concentrations of Hg^{2+} from 0-450 μM were added in all three breeds of Au NPs. The Au NPs gradually aggregated

with an increase in Hg^{2+} concentration supported by visible color change, are shown in Fig.S4. The absorption ratio (A_{LSPR}/A_{TSPR}) of UV-Vis spectroscopic LSPR and TSPR peaks have been used to demonstrate aggregation of NPs. Accordingly, the ratio of absorption values namely, (A_{740}/A_{566}), (A_{746}/A_{554}) and (A_{707}/A_{540}) of all three kinds of Au NPs were used respectively.

As shown in Fig. 8, in all three cases, an increase in Hg^{2+} leads to a noticeable change in A_{LSPR}/A_{TSPR} values. Here, fitting range is from 0 to 450 μM with a Boltzmann sigmoidal equations have regression coefficients $R^2_{(16\text{-}2\text{-}16)\ Au}$ = 0.98897 (Y = 0.774 – 0.9357 (1 + *exp* (X-51.260)/ 55.143)), $R^2_{(18\text{-}2\text{-}18)\ Au}$ = 0.99264 (Y = 0.9742 – 2.316 (1 + *exp* (X-57.186)/ 99.848)) and $R^2_{(20\text{-}2\text{-}20)\ Au}$ = 0.98196 (Y = 0.6837 – 12.67112 (1 + *exp* (X-580.130)/ 172.177)), where Y is absorption ratio and X is the concentration of Hg^{2+}, respectively. In addition, a linear relationship exists between absorbance ratio and Hg^{2+} concentration from 0 to 60 μM with $R^2_{(16\text{-}2\text{-}16)\ Au}$ = 0.97342($Y = 0.00361X + 0.10587$), $R^2_{(18\text{-}2\text{-}18)\ Au}$ = 0.99522 ($Y = 0.00547X + 0.13695$) and $R^2_{(20\text{-}2\text{-}20)\ Au}$ = 0.97803 ($Y = 0.00219X + 0.26002$),have been presented in inset of Fig. 8. The limit of detection (LOD) for Hg^{2+} based on $3\sigma/S$ for Au NPs synthesized with TTS of different chain length (m = 16, 18, 20) at a signal-to-noise ratio of 3 was estimated to be 0.107, 0.076 and 0.176 μM where σ *is* standard deviation and S is slope, respectively. The LODs of (18-2-18) Au was best in comparison to Au NPs synthesized by other surfactants. Also, the LOD was very much close to the Hg^{2+} detection limit set by world health organization (30 nM) and the U.S. environmental protection agency (10 nM).[48-50]

The response of all sensors was also analyzed by estimating the change in absorbance ratio as a function of time. Figures 8(a), 8(b) and 8(c) show the UV-Vis spectra of the Au NPs in the presence of Hg^{2+} taken after 24 min; UV-Vis spectra of Au NPs in the absence of metal ions are included for a comparison. Evidently, the both absorbance at TSPR and LSPR changed

significantly. The inset in the respective Figures 8(a), 8(b) and 8(c) before and after addition of Hg^{2+} displays visible color change indicative of Hg^{2+} detection. Predominantly, a noticeable shift in TSPR wavelength was observed for (18-2-18) Au NPs compared to other TTS capped NPs. The time dependent UV-Vis spectra for all three kinds of Au nanoparticles in the presence of Hg^{2+} are shown in Fig. S5 and the corresponding absorbance ratios are summarized in Fig. 9(d). A sharp change in absorbance ratio was observed in less than 3 min followed by nearly similar absorbance ratio values. Principally, the (18-2-18) Au NPs exhibited large absorbance change compared to other Au NPs, which indicates that triangular shaped Au NPs are promising for faster detection of Hg^{2+}.

The Au NPs can detect of Hg^{2+} when it exists in Hg^0state.[51,52] The mercury in Hg^{2+} state is not capable to interact with Au, thus cannot be detected. Only reduced form of mercury (Hg^0) possess the distinctive property of amalgamation with Au, and give response in term of change in absorption ratio (A_{LSPR}/A_{TSPR}), color and aggregation of Au NPs. Therefore, availability of a reducing agent is desired on the Au surface; the citrate ion in the present case seems to resolve that tenacity. Presence of citrate ions is likely to complete reduction of Hg^{2+} and allow propagation of Au-Hg alloy.[53,54] According to previous studies, the lower energy (111) plane of triangular and hexagon Au NPs are more prone towards incoming moiety.[55-57] Therefore, it is reasonable to say that Hg^0 will adsorb preferentially on the (111) plane of NPs. Elevated adsorption of Hg^0 can be expected when percentage of triangular shape particles are on higher side. Here, the anisotropic Au NPs synthesized with (18-2-18) were most sensitive towards Hg^{2+} than the NPs synthesized with other TTS. The presence of more number of triangular Au NP is probably the intention for better detection capability than other Au NPs.

Further, the selectivity of (18-2-18) Au NPs was investigated in comparison to the wide range of metal ions including Hg^{2+}, Ru^{3+}, Pb^{2+}, Sn^{2+}, Ni^{2+}, Cu^{2+}, Zn^{2+}, Mn^{2+} and Cd^{2+}.The absorbance ratio of different metal ions taken under similar conditions and corresponding images have been shown in Fig.9. Clearly, the Au NPs were most sensitive and exhibited higher selectivity towards Hg^{2+} compared to other metal ions. The inset figure shows the absorbance ratio of all Au NPs before and after addition of Hg^{2+}, whereby propagating that (18-2-18) plugged Au NPs revealed maximum absorbance change compared to other TTS capped NPs, indicating that triangular shaped Au NPs with truncated corner are promising for Hg^{2+} detection.

4. Conclusions

The effect of TTS with different hydrocarbon chain length on the growth of Au NPs was thoroughly investigated as function of their concentrations. The Au NPs were synthesized using TTS (m =16, 18, 20) in range from 0.10 to 5 mM concentrations. The hydrocarbon chain length and their concentration significantly influenced the shape and size of Au NPs. The TTS (18-2-18) promotes growth of Au NPs with triangular shape. In addition, the presence of more number of triangular shaped NPs have been found effective for detection Hg^{2+}. The results suggest that the TTS act as shape directing agent for growth of Au NPs. Therefore, optimization of change length is important for obtaining desire shaped NPs. To the best of our knowledge via thermal reduction method, the Au NPs, we didn't encounter any literature where TTS with higher tail length have been used to design well defined morphologies. Moreover, one of the surfactant demonstrates decent levels of Hg sensing capabilities, which could be novelty of the present work.

Acknowledgement

The authors are indebted to the Vice Chancellor, Shoolini University of Biotechnology & Management Sciences, Solan, India for providing basic laboratory amenities.

Notes and references

1 Li. N. Zhao and P. D. Astruc, *Angew. Chem. Int. Ed.*, 2014, **53**, 1756-1789.

2 Y. Xia, Y. Xiong, B. Lim and S. E. Skrabalak, *Angew. Chem. Int. Ed*., 2009, **48,** 60-103.

3 H. M. Chen, R. S. Liu, M. Y. Lo, S. C. Chang, L. D. Tsai, Y. M. Pengand J. F. Lee, *J. Phys. Chem. C,* 2008, **112,** 7522-7526.

4 N. R. Jana, L. Gearheart and C. J. Murphy, *J. Adv. Mater.*, 2001, **13,** 1389-1393.

5 J. Hu, T. W. Odom and C. M. Lieber, *Acc. Chem. Res*., 1999, **32,** 435-445.

6 X. Sun, S. Dong and E. Wang, *Angew. Chem. Int. Ed.,* 2004, **43,** 6360-6363.

7 M. S. Bakshi, F. Possmayer and N. O. Petersen, *J. Phys. Chem. C,* 2007, **111,** 14113-14124.

8 S. Shankar, A. Rail, B. Ankamwar, A. Singh, A. Ahmad and B. Sastry, *Nat. Mater.,* 2004, **3**, 482-488.

9 J. Xie, J. Y. Lee and I. C. D. Wang, *J. Phys. Chem. C,* 2007, **111**, 10226-10232.

10 N. Zhao, Y. Wei, N. Sun, Q. Chen, J.Bai, L. Zhou, Y. Qin, M. Li and L. Qi, *Langmuir,* 2008, **24**, 991-998.

11 B. Wiley, Y. Sun and Y. Xia, *Acc. Chem. Res.,* 2007, **40***,* 1067-1076.

12 M. Murawska, M. Wiatr, P. Nowakowski, K. Szutkowski, A. Skrzypczak and M. Kozak, *Radiat. Phys. Chem.,* 2013, **93**, 160-167.

13 D. Jamwal, G. Kaur, P. Raizada, P. Singh, D. Pathak and P.Thakur, *J.Phys. Chem. C,* 2015, **119**, 5062-5073.

14 T. Jain, R. Ali, T. Bagha, H. Shekhar, R. Crawford, E. Johnson, K. Norgaard, K. Holmberg, P. Erhartcand K. M. Poulsen, *J. Mater. Chem.* C, 2014, **2**, 994-1003.

15 S. G. Grana, J. P. Juste, R. A. A. Puebla, A. G. Martinez and L. M. M. Marzan, *Adv. Optical Mater.,* 2013, **1**, 477-481.

16 M. S. Bakshi, F. Possmayer and N. O. Petersen, *J. Phys. Chem. C,*2008, **112,**8259-8265.

17 M. S. Bakshi, P. Thakur, S. Sachar and T. S. Banipal, *Mater. Lett.,* 2007, **61**, 3762-3767.

18 J. Xu, J. Hu, C. Peng, H. Liu and Y. Hu, *J. Colloid Interface Sci.,*2006, **298**, 689-693.

19 J. Xu, X. Han, H. Liu and Y. Hu, *J. Dispersion Sci. Technol.,*2005, **26**, 473-476.

20 W. Wang, Y. Han, M.Gao and Y. Wang, *J. Nanopart. Res.,* 2013, **15**, 1380.

21 W. Li, C. Sun, B. Hou and X. Zhou,*Int. J. Spectrosc.,*2012, **2012**, 1-7.

22 L. Chen, Y. Shang, H. Liu and Y. Hua, *Mater. Des.* 2010, **31**, 1661-1665.

23 M. S. Bakshi, S. Sachar, G. Kaur, P. Bhandari, G. Kaur, M. C. Biesinger, F. Possmayer and N. O. Petersen, *Cryst. Growth Des.,* 2008, **8**,1713-1719.

24 A. G. Martnez, J. P. Juste, E. C. Argibay, G. Tardajos and L. M. Marz, *Angew. Chem. Int. Ed.,* 2009, **48**, 9484-9488.

25 Q. Liu, M. Guo, Z.Nie, J. Yuan, J. Tan and S. Yao, *Langmuir,* 2008, **24***,* 1595-1599.

26 F. Xu, Q. Zhang andZ. Gao, *Colloids Surf A Physicochem Eng Asp.,*2013, **417**, 201-210.

27 M. S. Bakshi, P. Thakur, P. Khullar, G. Kaur and T. S. Banipal, *Cryst. Growth Des.,* 2010, **10**, 1813-1822.

28 M. S. Bakshi, P. Thakur, S. Sachar, G. Kaur, T. S. Banipal, F. Possmayer and N. O. Petersen, *J. Phys. Chem. C,*2007, **111***,* 18087-18098.

29 A. R. Tao, H. Susan and P. Yang, *Small*, 2008, **4,** 310-325.

30 J. Du, B. Zhu and X. Chen, *Small,* 2013, **9**, 24, 4104-4111.

31 Y. Jiang, H. Zhao, N. Zhu, Y. Lin, P. Yu and L. Mao, *Angew. Chem. Int. Ed.,* 2008, **47**, 8601-8604.

32 B. Kong, A. Zhu, Y. Leo, Y. Tian, Y. Yu and G. Shi. *Angew Chem Int. Ed.,* 2011, **50,** 1837-1840.

33 C. D. Medley, J. E. Smith, Z. W. Tang, Y. R. Wu, S. Bamrungsap and W. H. Tan, *Anal. Chem.,* 2008, **80**, 1067-1072.

34 Y. Zhang, B. Li and C. Xu, *Analyst,* 2010, **135**, 1579-1584.

35 K. Ai, Y. Liu and L. Lu, *J Am. Chem. Soc.,* 2009,**131**, 9496-9497.

36 C. Dwivedi, A. Chaudhary, A. Gupta and C. K. Nandi, *ACS Appl. Mater. Interfaces,* 2015, 7, 5039-5044.

37 A. Singh, R. Pasrichax and M. Sastry, *Analyst,* 2012, **137**, 3083-3090.

38 L. Chen, X. Fu, W. Lu and L. Chen, *ACS Appl. Mater. Interfaces,* 2013, **5**, 284-290.

39 S. D. Wettig and R. E. Verrall, *J. Colloid Interface Sci*., 2001, **235**, 310-316.

40 W. L. Manner, A. R. Bishop, G. S. Girolami and R. G. Nuzzo, *J. Phys. Chem. B,*1998, **102**, 8816-8824.

41 M. J. Hostetle, J. J. Stokes and R.W. Murray, *Langmuir,* 1996, **12**, 3604-3612.

42 H. Li and C. P. Tripp, *Langmuir,* 2002, **18**, 9441-9446.

43 I. Zawisza, X. Bin and J. Lipkowski, *Langmuir,* 2007*,* **23***,* 5180-5194.

44 J. F. Liu and W. A. Ducker,*J. Phys. Chem. B,* 1999, **103***,* 8558-8567.

45 Y. Liang, D. Wu, X. Feng and K. Mullen, *Adv. Mater*., 2009, **21**, 1679-1683.

46 J. C. Love, L. A. Estroff, J. K. Kriebel, R. G. Nuzzo and G. M. Whitesides, *Chem. Rev.,* 2005, **105,** 1103-1169.

47 O. M. Magnussen, *Chem. Rev*., 2002, **102**, 679-726.

48 G. H. Chen, W. Y. Chen, Y. C. Yen, C. W. Wang, H. T. Chang and C. F. Chen, *Anal. Chem.,* 2014, **86**, 6843-6849.

49 G. J. Burin and G. C. Becking, *Trace substances in environmental health—XXIV*, 1991, 207-219.

50 R. K. Srivastava, J. E. Staudt and W. Jozewicz, *Environ. Prog.,* 2005, **24,** 198-213.

51 K. Leopold, M. Foulkes and P. J. Worsfold, *Anal. Chem.,* 2009, **81**, 3421-3428.

52 T. Lou, Z. Chen, Y. Wang and L. Chen, *ACS Appl. Mater. Interfaces,* 2011, **3**, 1568-1573.

53 I. O. Jimenez, X. Lopez, J. Arbiol andV. Punte, *ACS Nano,* 2012, **6**, 2253-2260.

54 C. Lin, Y. C. J. Yu, Y. H. Lin and W. L. Tseng, *Anal. Chem.,* 2010, **82***,* 6830-6837.

55 Y. Xia, J. Ye, k. Tan, J. Wang and G. Yang, *Anal Chem.,* 2013, **85**, 6241-6247.

56 Z. Chen, T. Lou, Q. Wu, K. Li, L. Tan and J. Sun, *Sensors and Actuators B,* 2015, **221**, 365-369.

57 A. Chaudhary, C. Dwivedi, M. Chawla, A. Gupta and C. K. Nandi, *J. Mater. Chem. C*, 2015, **3,** 6962-6965.

Tables and Figure captions

Scheme 1 Au NPs growth mechanism involving various surfactants (*m* = 16, 18, 20).

Table 1 Peak assignment of TTS (*m* = 16, 18, 20) in the presence and absence of Au NPs.

Table 2 Particle size distribution of Au NPs synthesized with different TTS (*m* = 16, 18, 20).

Fig. 1 (a), (c) & (e) demonstrating UV-Vis absorption spectra of Au NPs at different concentrations (0.10-5mM) of surfactants (16-2-16), (18-2-18) and (20-2-20) respectively. (b), (d) & (f) represent the wavelength/intensity versus concentration plot for (16-2-16), (18-2-18) and (20-2-20) respectively.

Fig. 2 Comparative plot of UV-Vis absorption spectra of Au NPs synthesized with 4 mM of different TTS (*m* = 16, 18, 20).

Fig. 3 TEM images of Au NPs at (a) 0.10 and (c) 4 mM of (16-2-16). (b) & (d) show histograms of particle size distribution.(e) Magnified TEM image of Au NPs. (f) High-magnification image of single particle capped with surfactant layer of thickness ~1.4 nm. (g) Line profile and (h) EDX spectrum of Au NPs.

Fig. 4 TEM images of Au NPs synthesized with (a) 0.10 and (c) 4 mM of (18-2-18) and histograms showing particle shape distribution in (b) and (d). (e) and (f) Magnified TEM image of Au NPs. (g) and (h) High-magnification image of single particle capped surfactant layer of thickness ~1.7 nm taken from (f).

Fig. 5 TEM images of Au NPs synthesized with (a) 0.10 and (c) 4 mM of (20-2-20) and histograms showing particle shape distribution in (b) and (d). (e) Magnified TEM

image of Au NPs and (f) high-magnification image of Au NP showing surfactant layer of thickness ~1.1 nm taken from (e).

Fig. 6 FTIR spectra of Au NPs synthesized with 4 mM of different TTS (*m* = 16, 18, 20).

Fig. 7 Plots of A_{LSPR}/A_{TSPR} versus concentrations of Hg^{2+}range from 0 to 450 μM in 0.01 M sodium acetate at pH=4 for Au NPs synthesized with different TTS (*m* = 16, 18, 20). The inset is the plot for concentrations of Hg^{2+} range from 0 to 60 μM.

Fig. 8 UV-Vis spectra ofAu NPs synthesized with different TTSin presence and absence of Hg^{2+}after 24 min: (a) (16-2-16), (c) (18-2-18) and (e) (20-2-20). The inset photographs shows the corresponding state of Au NPs(d) Plots of A_{LSPR}/A_{TSPR} versus time for different Au NPs for detection of Hg^{2+}.

Fig. 9 Plots of A_{LSPR}/A_{TSPR} of (18-2-18) Au NPs for different metal ions under similar conditions with corresponding photographs. The concentration of all metal ions was 450 μM. The inset is the comparison plot of A_{LSPR}/A_{TSPR} of all three kinds of Au NPs in the presence and absence of Hg^{2+}.

Electronic Supplementary Material

Fig.S1 UV-Vis absorption spectra of Au NPs synthesized without TTS.

Fig.S2 Histograms showing size distribution of Au NPs synthesized with 0.10 mM and 4mM of different TTS: (a), (b) (16-2-16), (c), (d) (18-2-18) and (e), (f) (20-2-20).

Fig.S3 FTIR spectra of pure TTS (*m* = 16, 18, 20).

Fig.S4 Photographs of all three varieties of Au NPs with different concentrations of Hg^{2+} range from 0 to 450 μM.

Fig.S5 Time dependent UV-Vis spectra ofAu NPs synthesized with different TTS in presence of Hg^{2+}: (a) (16-2-16) Au NPs, (c) (18-2-18) Au NPs and (e) (20-2-20) Au NPs.

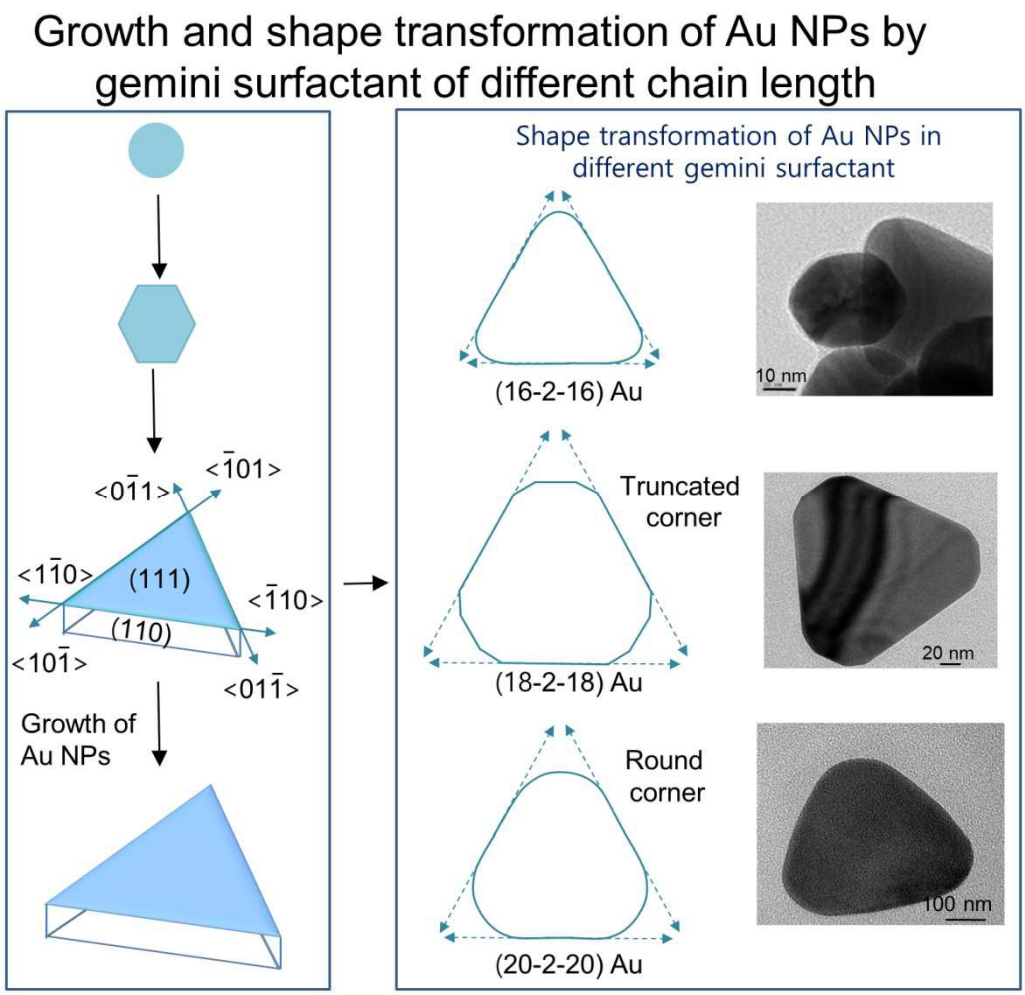

Scheme 1 Growth of Au NPs by different TTS (*m* = 16, 18, 20).

Table 1 Peak assignment of TTS (m = 16, 18, 20) in the presence and absence of Au NPs.

Peak assignment	(16-2-16)	(16-2-16)-Au	(18-2-18)	(18-2-18)-Au	(20-2-20)	(20-2-20)-Au
ν_{sym} (C-H)	2854	2854	2854	2854	2854	2854
ν_{asym} (C-H)	2921	2925	2921	2921	2921	2921
□s (C-H)	1469	1473	1473	1477	1473	1477
	1395	1398	11394	1395	1398	1395
ρ_{asym} (NR_4^+)	1640	1659	1640	1659	1640	1659
	--	1585	--	1573	--	1573
ν (C-N^+)	1154	1160	1166	1138	1130	1138
	1067	1082	1072	1082	1080	1082
	978	955	981	940	970	955
	907	911	911	922	907	925
	855	847	855	840	855	844
$\rho_w(CH_2)_n$	1302	1309	1305	1298	1302	1298
$\rho_t(CH_2)_n$	1268	1275	1265	1261	1268	1268
$\rho_r(CH_2)_n$	724	728	724	729	724	727

ν = stretching, sym = symmetric, asym = antisymmetric, □s = methylene scissoring, ρ_r = rocking, ρ_t = twisting, ρ_w = wagging.

Table 2 Particle size distribution of Au NPs synthesized with different TTS (*m* = 16, 18, 20).

Twin tail surfactant	Concentration (mM)	Average particle size (nm)	Average size of particles with different shapes (nm)					
			Round	Triangular	Rectangular	Pentagon	Hexagon	Rod
(16-2-16)	0.10	39.6±13.0	34.6±10.3	61.6±5.3	----	53.4±7.2	38.6±7	---
	4.0	54.8±25.5	35.1±12.4	62.1±25.1	59.3±3.6	55.5±3.5	40.6±5.3	76±42.6
(18-2-18)	0.10	66.6±36.5	48.4±16.4	148±26.5	----	58.2±4.3	73.2±6.2	---
	4.0	138.4±71.4	69.6 ±8.5	219.7±37.8	186.3	93.9	79.9 ±3.4	173.8
(20-2-20)	0.10	42.6 ±17.7	32.4±6.2	54.1±18.2	46.1±16.1	51.2±6.7	33.3±12	---
	4.0	54.8±30.9	37.8 ±12.3	68.9±29.9	59.9±16.1	64.9 ±16.5	40.8 ±15.3	---

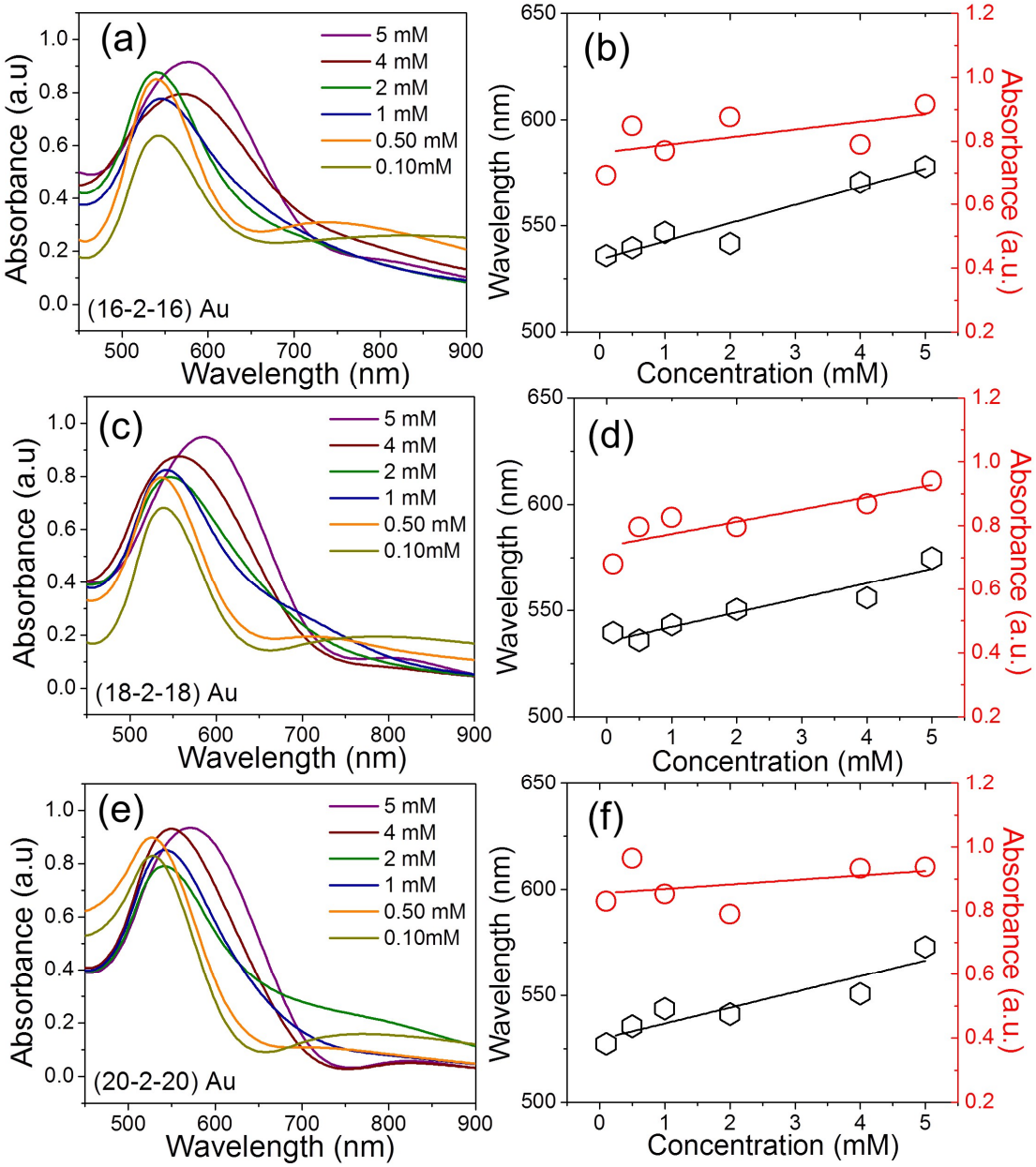

Fig.1 (a),(c)&(e) demonstrating UV-Vis absorption spectra of Au NPs at different concentrations (0.10-5mM) of surfactants (16-2-16), (18-2-18) and (20-2-20) respectively. (b),(d)&(f) represent the wavelength/intensity versus concentration plot for (16-2-16), (18-2-18) and (20-2-20) respectively.

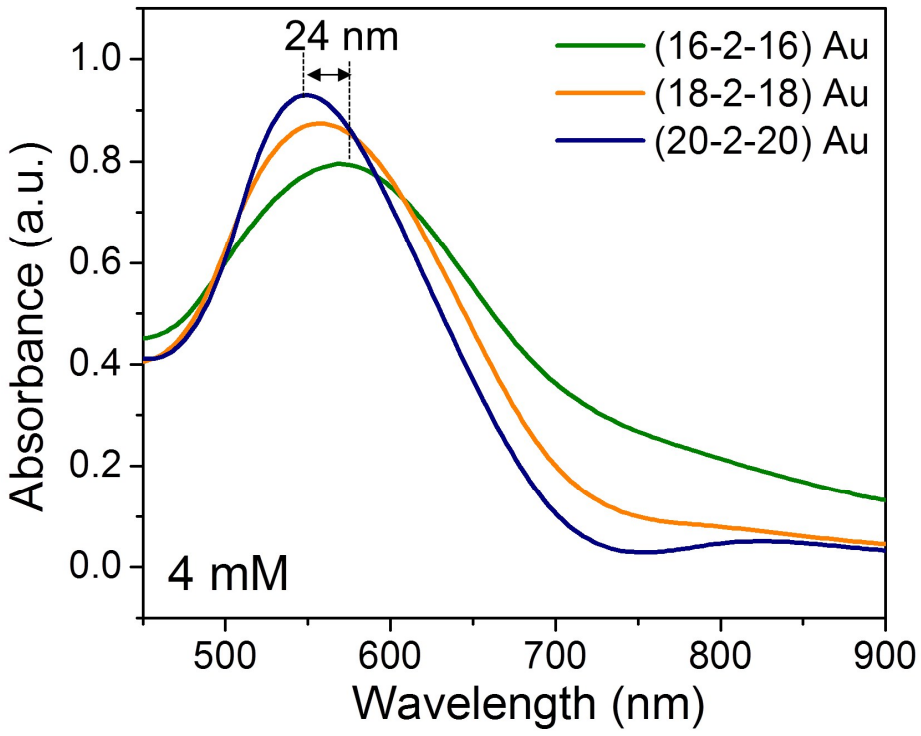

Fig.2 Comparative plot of UV-Vis absorption spectra of Au NPs synthesized with 4 mM of different TTS (m = 16, 18, 20).

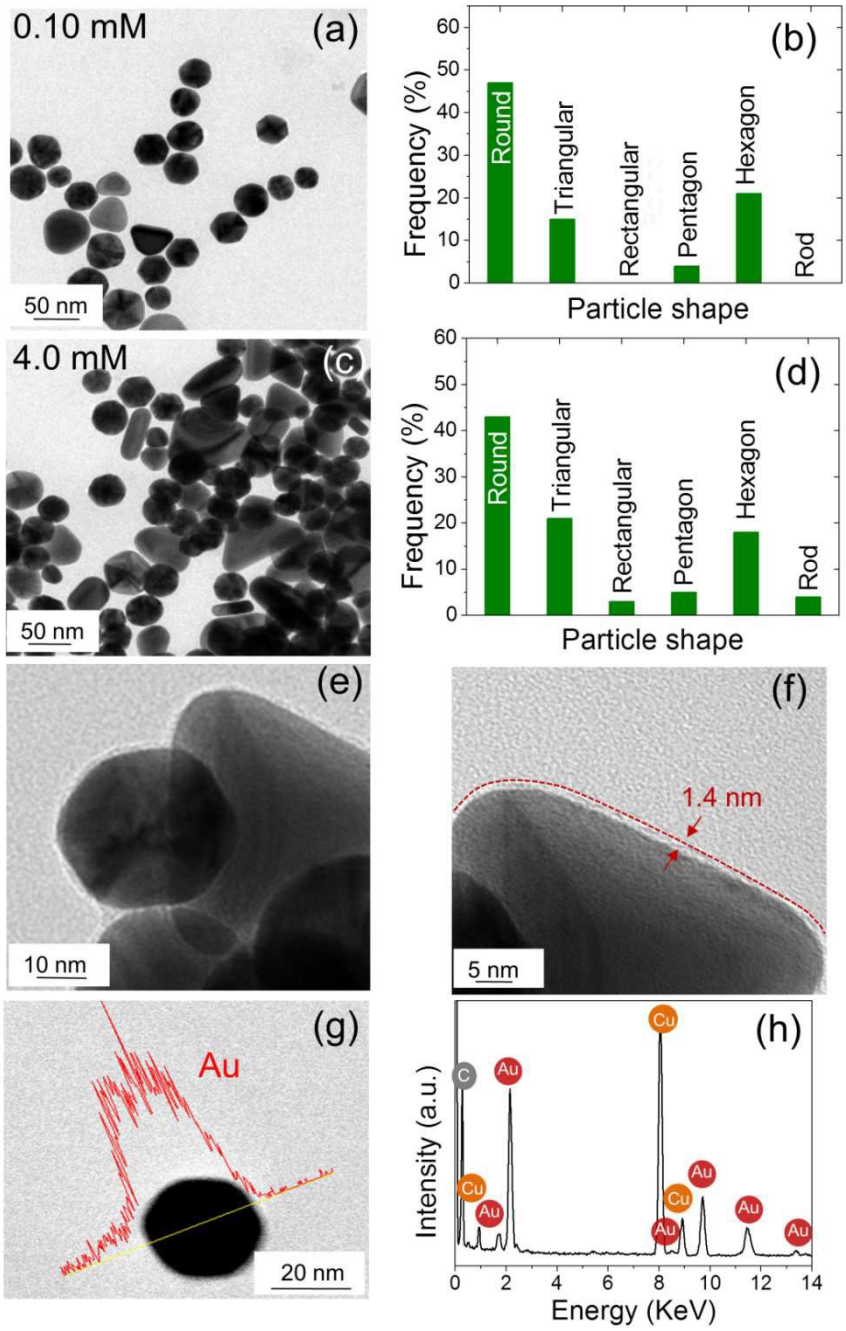

Fig. 3 TEM images of Au NPs at (a) 0.10 and (c) 4 mM of (16-2-16). (b) and (d) show histograms of particle size distribution. (e)Magnified TEM image of Au NPs. (f) High-magnification image of single particle capped with surfactant layer of thickness ~1.4 nm. (g) Line profile and (h) EDX spectrum of Au NPs.

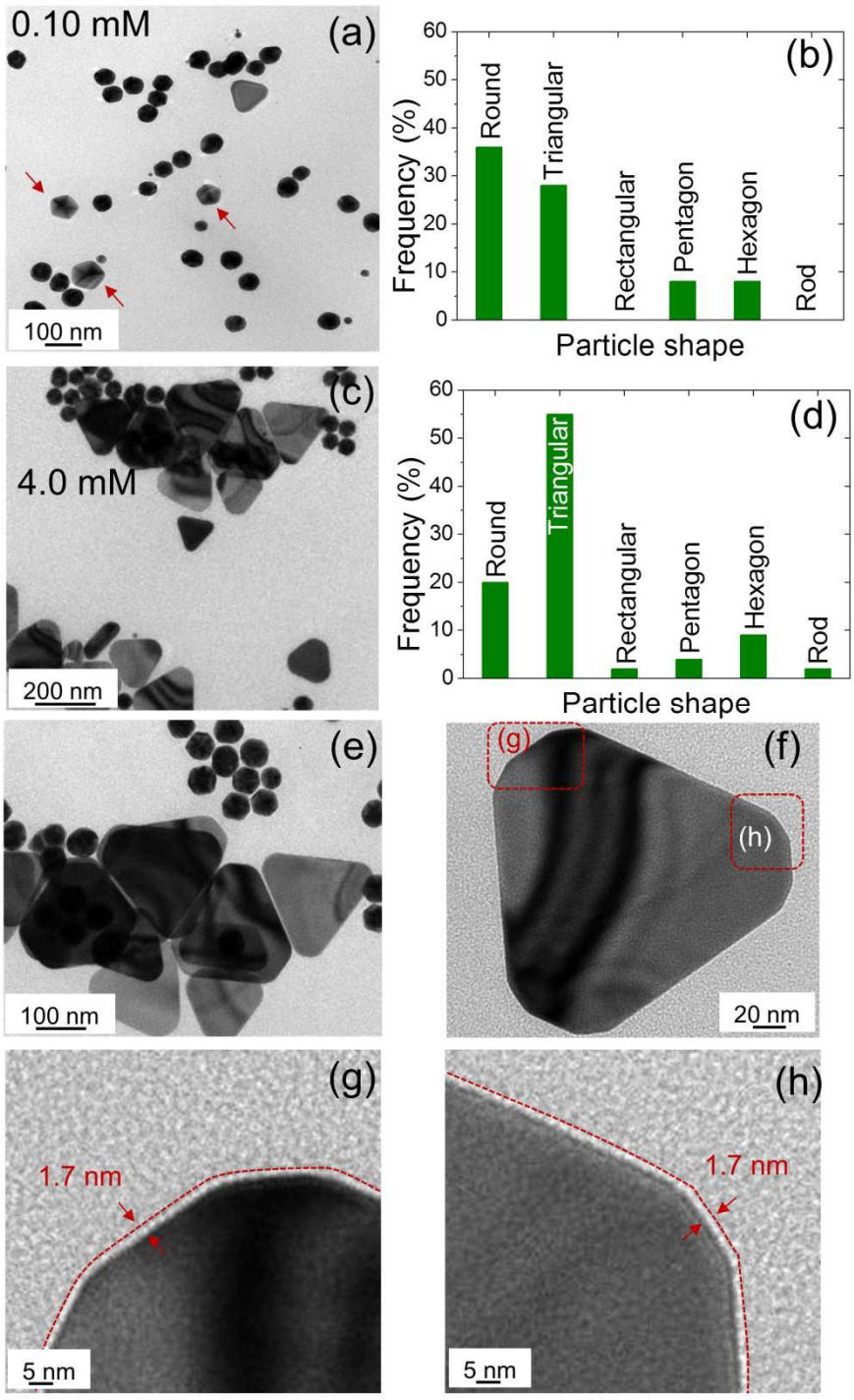

Fig. 4 TEM images of Au NPs synthesized with (a) 0.10 and (c) 4 mM of (18-2-18) and histograms showing particle shape distribution in (b) and (d). (e)and(f)Magnified TEM image of Au NPs. (g) and (h) High-magnification image of single particle capped surfactant layer of thickness ~1.7 nm taken from (f).

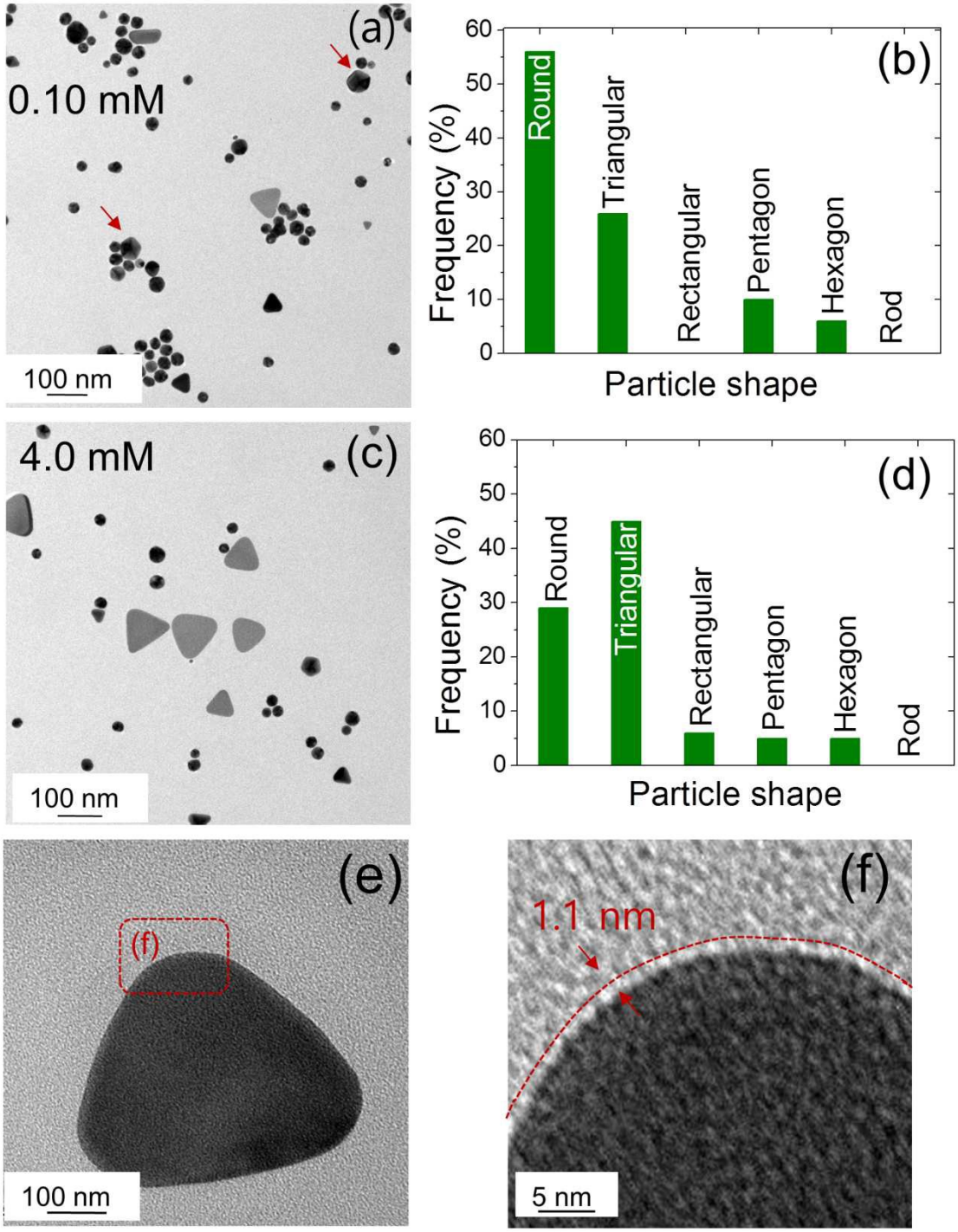

Fig. 5 TEM images of Au NPs synthesized with (a) 0.10 and (c) 4 mM of (20-2-20) and histograms showing particle shape distribution in (b) and (d). (e)Magnified TEM image of Au NPs and (f) high-magnification image of Au NP showing surfactant layer of thickness ~1.1 nm taken from (e).

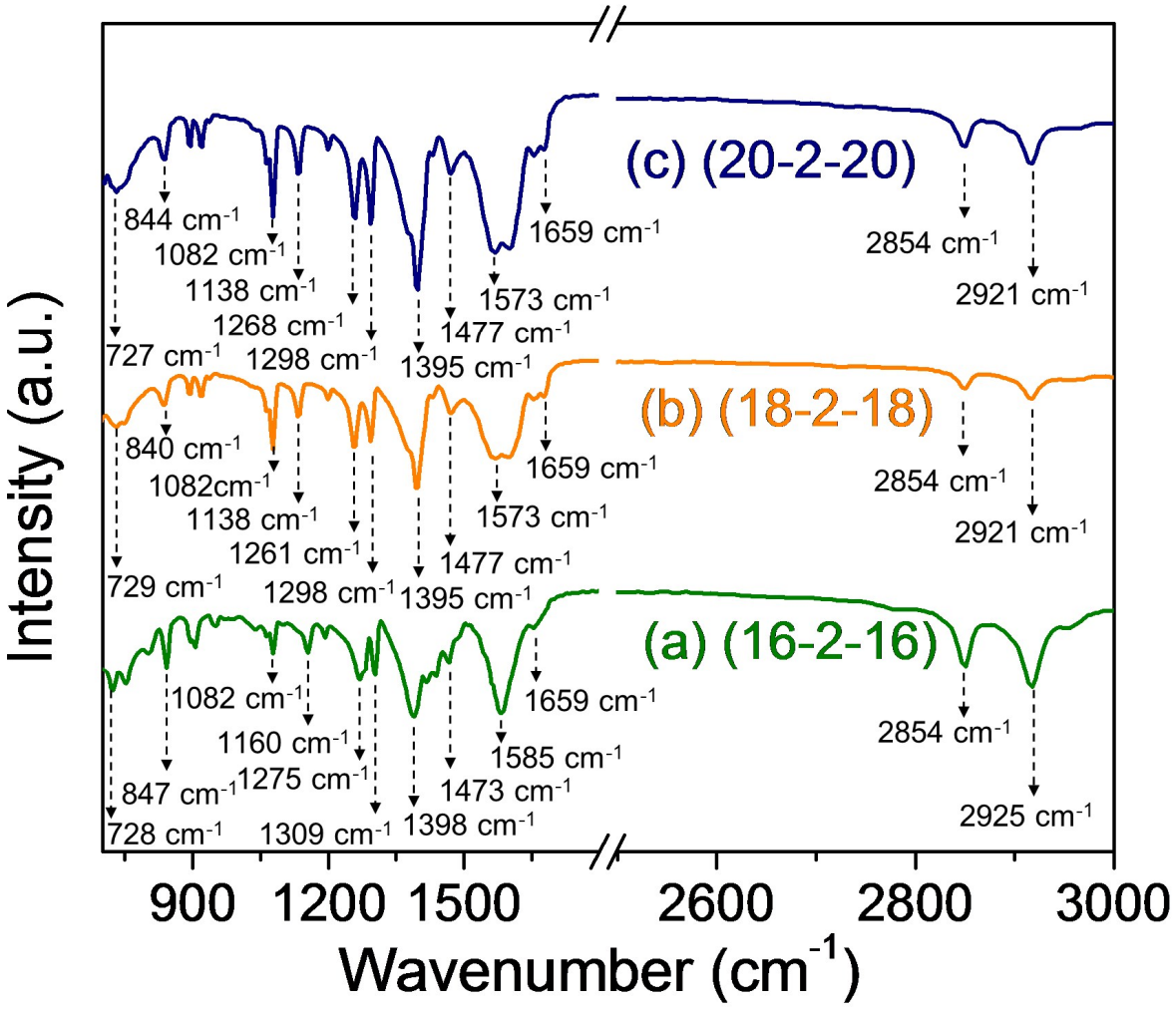

Fig.6 FTIR spectra of Au NPs synthesized with 4 mM of different surfactants

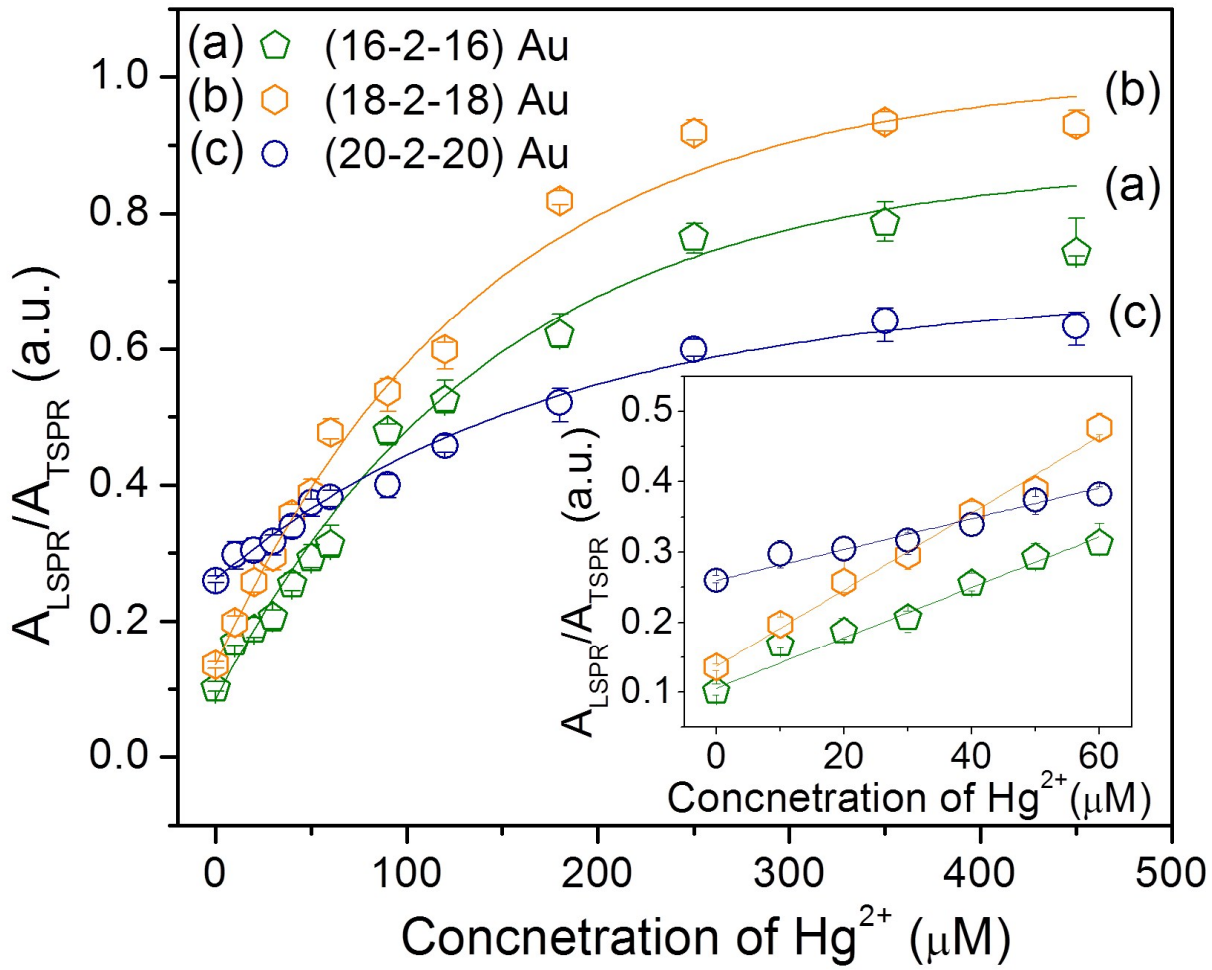

Fig.7 Plots of A_{LSPR}/A_{TSPR} versus concentrations of Hg^{2+} range from 0 to 450 μM in 0.01 M sodium acetate at pH=4 for Au NPs synthesized with different TTS (*m* = 16, 18, 20). The inset is the plot for concentrations of Hg^{2+}range from 0 to 60 μM.

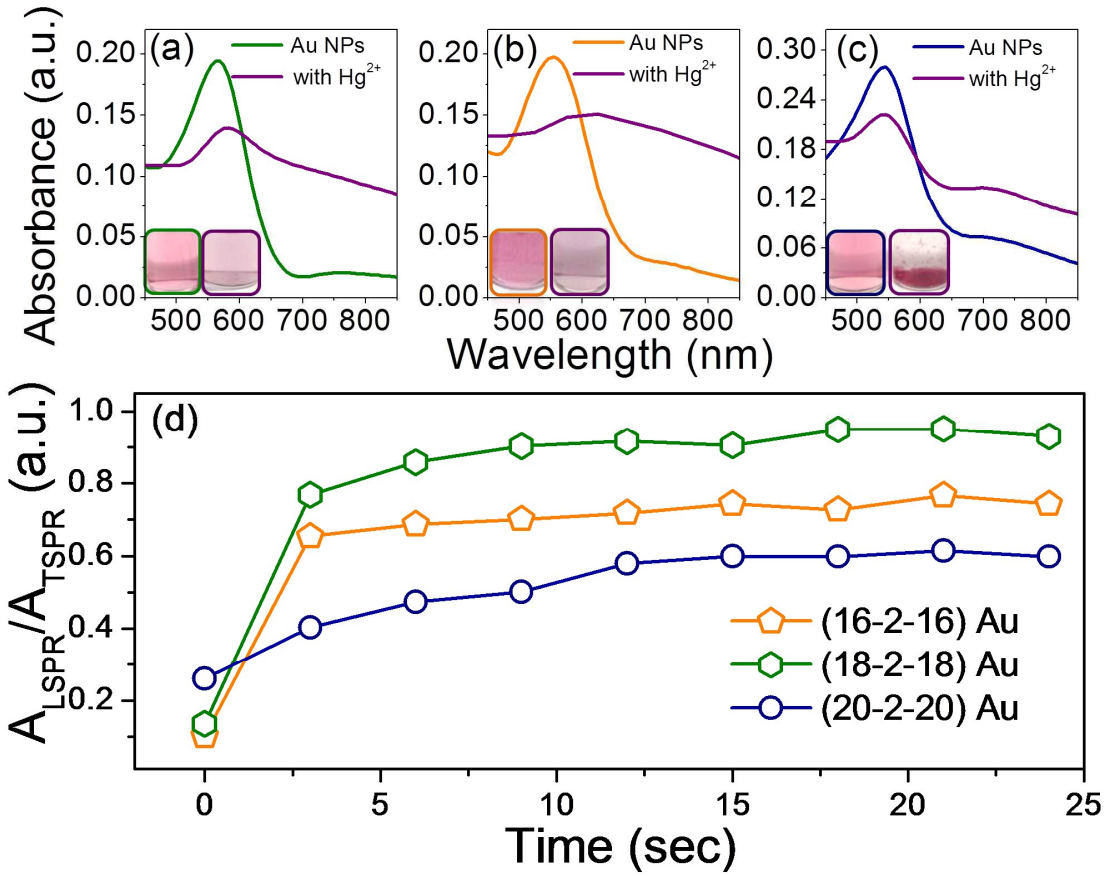

Fig.8 UV-Vis spectra of Au NPs synthesized with different TTS in presence and absence of Hg^{2+}after 24 min: (a) (16-2-16), (c) (18-2-18) and (e) (20-2-20). The inset photographs shows the corresponding state of Au NPs(d) Plots of A_{LSPR}/A_{TSPR} versus time for different Au NPs for detection of Hg^{2+}.

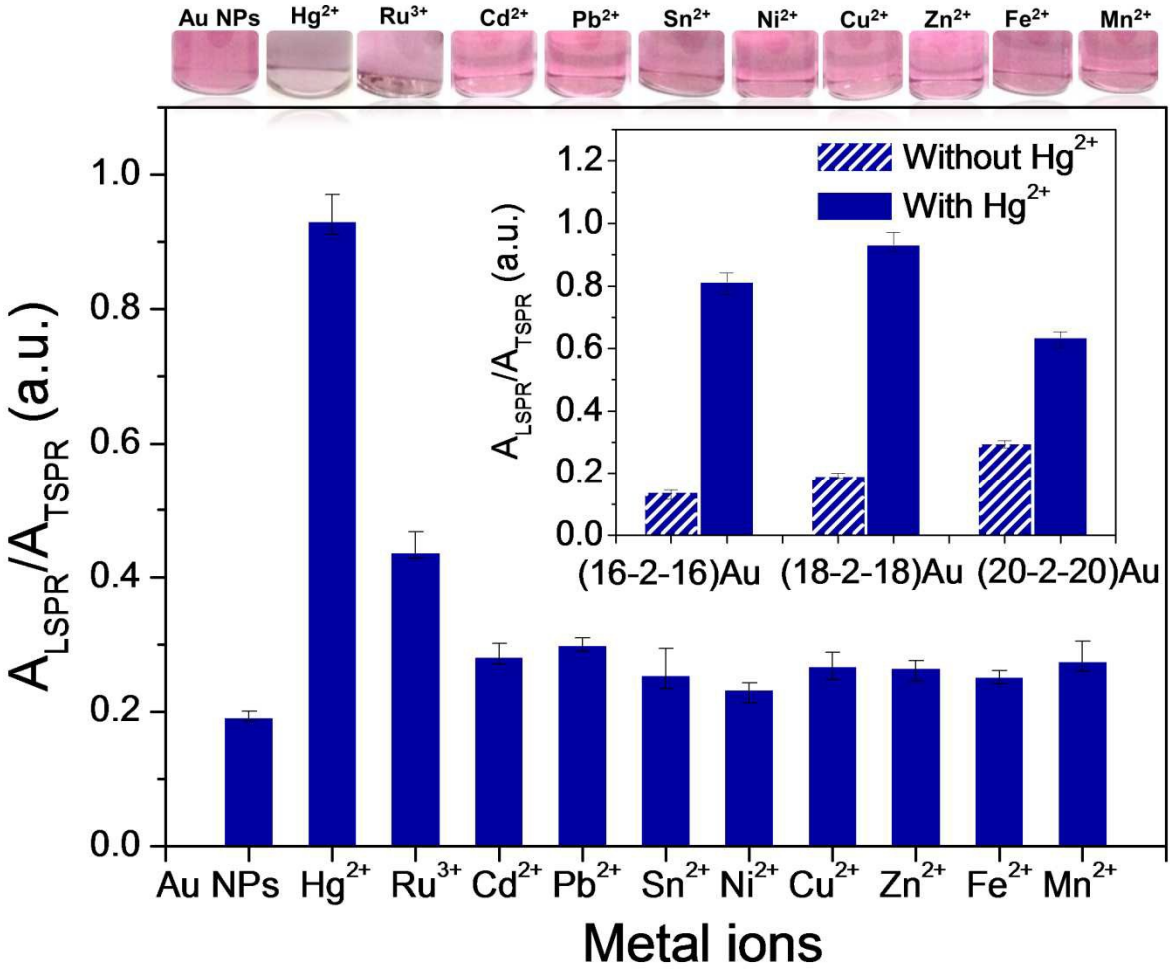

Fig.9 Plots of A_{LSPR}/A_{TSPR} of (18-2-18) Au NPs for different metal ions under similar conditions with corresponding photographs. The inset is the comparison plot of A_{LSPR}/A_{TSPR} of three varieties of Au NPs in the presence and absence of Hg^{2+}.